

GALILEO GALILEI (GG)

**SYSTEM PERFORMANCE
REPORT**

DRL/DRD: DEL-027

<i>Written by</i>	<i>Responsibility</i>
G. Catastini	Author
<i>Verified by</i>	
A. Anselmi	Checker
<i>Approved by</i>	
	Product Assurance
	Configuration Control
	Design Engineer
	System Engineering Manager
A. Anselmi	Study Manager
<i>Documentation Manager</i>	
R. Cavaglià	

The validations evidence are kept through the documentation management system.

ISSUE	DATE	§ CHANGE RECORDS	AUTHOR
Draft 1.0	03-03-09	First draft produced for IRR, circulated for comments	GC
1	12-03-09	IRR issue	
2	08-Jun-09	Issue submitted to PRR	

TABLE OF CONTENTS

1. SCOPE AND PURPOSE	5
2. REFERENCES	6
2.1 Applicable Documents	6
2.2 Standards	6
2.3 ASI Reference Documents	6
2.4 GG Phase A2 Study Notes	6
3. GG EXPERIMENT ERROR BUDGET	8
3.1 Error Budget Formulation	8
3.2 Experiment Environment	9
3.3 Error Budget	17

LIST OF FIGURES

FIGURE 3.2-1: NON-GRAVITATIONAL ACCELERATION IN THE IRF [X AXIS]9
FIGURE 3.2-2: NON-GRAVITATIONAL ACCELERATION IN THE IRF [Y AXIS]10
FIGURE 3.2-3: NON-GRAVITATIONAL ACCELERATION IN THE LHLV REFERENCE FRAME [X AXIS]11
FIGURE 3.2-4: NON-GRAVITATIONAL ACCELERATION IN THE LHLV REFERENCE FRAME [Y AXIS]12
FIGURE 3.2-5: NON-GRAVITATIONAL ACCELERATION IN THE LHLV REFERENCE FRAME [Z AXIS]13
FIGURE 3.2-6: NON-GRAVITATIONAL ACCELERATION IN THE LHLV REFERENCE FRAME AFTER DFAC AND DIFFERENTIAL
ACCELEROMETER COMMON MODE REJECTION [X AXIS]14
FIGURE 3.2-7: NON-GRAVITATIONAL ACCELERATION IN THE LHLV REFERENCE FRAME AFTER DFAC AND DIFFERENTIAL
ACCELEROMETER COMMON MODE REJECTION [Y AXIS]15
FIGURE 3.2-8: NON-GRAVITATIONAL ACCELERATION IN THE LHLV REFERENCE FRAME AFTER DFAC AND DIFFERENTIAL
ACCELEROMETER COMMON MODE REJECTION [Z AXIS]16
FIGURE 3.3-1: AMPLITUDE SPECTRUM OF THE TEST MASSES DIFFERENTIAL DISPLACEMENT DUE TO THE MAIN SYSTEMATIC
ERRORS VS. THE TARGET EP VIOLATION SIGNAL.18
FIGURE 3.3-2: DETAILED VIEW OF THE AMPLITUDE SPECTRUM OF THE MAIN SYSTEMATIC ERRORS.....19
FIGURE 3.3-3: MAGNITUDE OF THE ERRORS WITH THE SAME FREQUENCY SIGNATURE AS THE EP VIOLATION SIGNAL, AS
FUNCTION OF INTEGRATION TIME.20

1. SCOPE AND PURPOSE

This document is submitted in partial fulfilment of Work Package 1A-ADA of the GG Phase A2 Study. It provides the analysis of the GG system performance. For an experiment such as GG, the performance is synthesised by an error budget of the scientific measurement. The document provides the experiment error budget and the associated justification.

2. REFERENCES

2.1 Applicable Documents

- [AD 1] ASI, "Progetto Galileo Galilei-GG Fase A-2, Capitolato Tecnico", DC-IPC-2007-082, Rev. B, 10-10-2007 and applicable documents defined therein

2.2 Standards

- [SD 1] ECSS-M-00-02A, Space Project Management – Tailoring of Space Standards, 25 April 2000
- [SD 2] ECSS-E-ST-10C, Space Engineering - System Engineering General Requirements, 6 March 2009
- [SD 3] ECSS-E-10-02A, Space Engineering – Verification
- [SD 4] ECSS-Q-00A, Space Product Assurance - Policy and Principles, and related Level 2 standards.

2.3 ASI Reference Documents

- [RD 1] GG Phase A Study Report, Nov. 1998, revised Jan. 2000, available at: <http://eotvos.dm.unipi.it/nobili/ggweb/phaseA/index.html>
- [RD 2] Supplement to GG Phase A Study (GG in sun-synchronous Orbit) "Galileo Galilei-GG": design, requirements, error budget and significance of the ground prototype", A.M. Nobili et al., Physics Letters A 318 (2003) 172–183, available at: http://eotvos.dm.unipi.it/nobili/documents/generalpapers/GG_PLA2003.pdf
- [RD 3] A. Nobili, DEL001: GG Science Requirements, Pisa, September 2008

2.4 GG Phase A2 Study Notes

- [RD 4] SD-RP-AI-0625, GG Final Report / Satellite Detailed Architecture Report, Issue 1
- [RD 5] SD-RP-AI-0626, GG Phase A2 Study Executive Summary, Issue 1
- [RD 6] SD-TN-AI-1163, GG Experiment Concept and Requirements Document, Issue 3
- [RD 7] SD-RP-AI-0620, GG System Performance Report, Issue 2
- [RD 8] SD-TN-AI-1167, GG Mission Requirements Document, Issue 2
- [RD 9] SD-RP-AI-0590, GG System Concept Report (Mission Description Document), Issue 3
- [RD 10] SD-SY-AI-0014, GG System Functional Specification and Preliminary System Technical Specification, Issue 1
- [RD 11] SD-RP-AI-0631, GG Consolidated Mission Description Document, Issue 1
- [RD 12] SD-TN-AI-1168, GG Mission Analysis Report, Issue 2
- [RD 13] DTM, GG Structure Design and Analysis Report, Issue 1

-
- [RD 14] SD-RP-AI-0627, GG Thermal Design and Analysis Report, Issue 1
 - [RD 15] SD-RP-AI-0268, GG System Budgets Report, Issue 1
 - [RD 16] SD-RP-AI-0621, Technical Report on Drag and Attitude Control, Issue 2
 - [RD 17] TL25033, Payload Architectures and Trade-Off Report, Issue 3
 - [RD 18] SD-RP-AI-0629, Technical Report on Simulators, Issue 1
 - [RD 19] ALTA, FEED Thruster Design and Accommodation Report, Issue 1
 - [RD 20] TASI-FI-44/09, Cold Gas Micro Thruster System for Galileo Galilei (GG) Spacecraft - Technical Report, Issue 1, May 2009
 - [RD 21] SD-RP-AI-0630, Spin Sensor Design, Development and Test Report, Issue 1
 - [RD 22] SD-TN-AI-1169, GG Launcher Identification and Compatibility Analysis Report, Issue 1
 - [RD 23] ALTEC-AD-001, GG Ground Segment Architecture and Design Report, Issue 1
 - [RD 24] SD-TN-AI-1218, GG Preliminary Product Tree, Issue 1
 - [RD 25] SD-PL-AI-0227, GG System Engineering Plan (SEP), Issue 2
 - [RD 26] TAS-I, Payload Development and Verification Plan, Issue 1
 - [RD 27] SD-PL-AI-0228, GG System Verification and Validation Plan, Issue 1
 - [RD 28] SD-TN-AI-1219, Report on Frequency Management Issues, Issue 1
 - [RD 29] SD-RP-AI-0632, GG Mission Risk Assessment And Mitigation Strategies Report, Issue 1
 - [RD 30] SD-RP-AI-0633, Report on Mission Costs Estimates, Issue 1

3. GG EXPERIMENT ERROR BUDGET

3.1 Error Budget Formulation

The mission goal of GG is testing the Equivalence Principle to 1 part in 10^{17} . In order to achieve the goal, numerous competing effects, which have nothing to do with a possible violation of the EP, must be kept by design below the stated experiment sensitivity. The analysis of these effects is reported in [RD 6], as organized in terms of seven experiment “drivers”:

1. the signal
2. external non gravitational forces
3. whirl motions
4. gravitational forces (earth tides)
5. satellite spin frequency
6. electro-magnetic coupling and other disturbing effects
7. temperature

Each driver, in turn, leads to derived requirements. The current definition of the requirements set is in [RD 6].

To prove that the stated requirement set is complete and sufficient, the GG simulator tool has been set up [RD 18]. The simulator provides a full simulation of the GG experiment, including a realistic description of the instrument, the spacecraft and the environmental effects, and all their interactions.

The simulator provides as output a time history of the relative displacements of the test cylinders under all the modelled environmental effects, plus an assumed EP-violation signal, at the orbit frequency $\nu_{EP} = 1.7538 \times 10^{-4}$ Hz in the inertial reference frame (IRF), of 0.6 pm magnitude (corresponding to the sensitivity of $\eta = 10^{-17}$). The purpose of the simulation is to show that, with the proper choice of the design parameters (the requirements), a violation signal of 0.6 pm magnitude can be detected and distinguished from the competing effects.

Chapter 3.2 below provides, in graphical form, a description of the external environmental acceleration environment and the effects of its suppression by the instrument common mode rejection and the spacecraft drag-free control.

3.2 Experiment Environment

The Figure 3.2-1 and Figure 3.2-2 provide the overall non gravitational acceleration (environment disturbances and s/c-PGB suspension force) sensed from the satellite centre of mass wrt. the inertial reference frame. The environmental forces are computed by using the MSIS '86 atmospheric model for the computation of the air density, temperature and chemical composition along the satellite orbit. The F10 and F10.B indexes related to the Solar activity and the Geomagnetic indexes Ap and Kp are used to feed the MSIS model. The solar radiation pressure and Earth albedo are computed modeling the satellite surface as a set of one cylinder and two simple flat surfaces.

The mean value of each acceleration component has been reported in the picture as a black line at the frequency $2 \cdot 10^{-6}$ Hz. In the IRF, the main component of the acceleration is at the orbit frequency, i.e. at the same frequency of the EP violation signal.

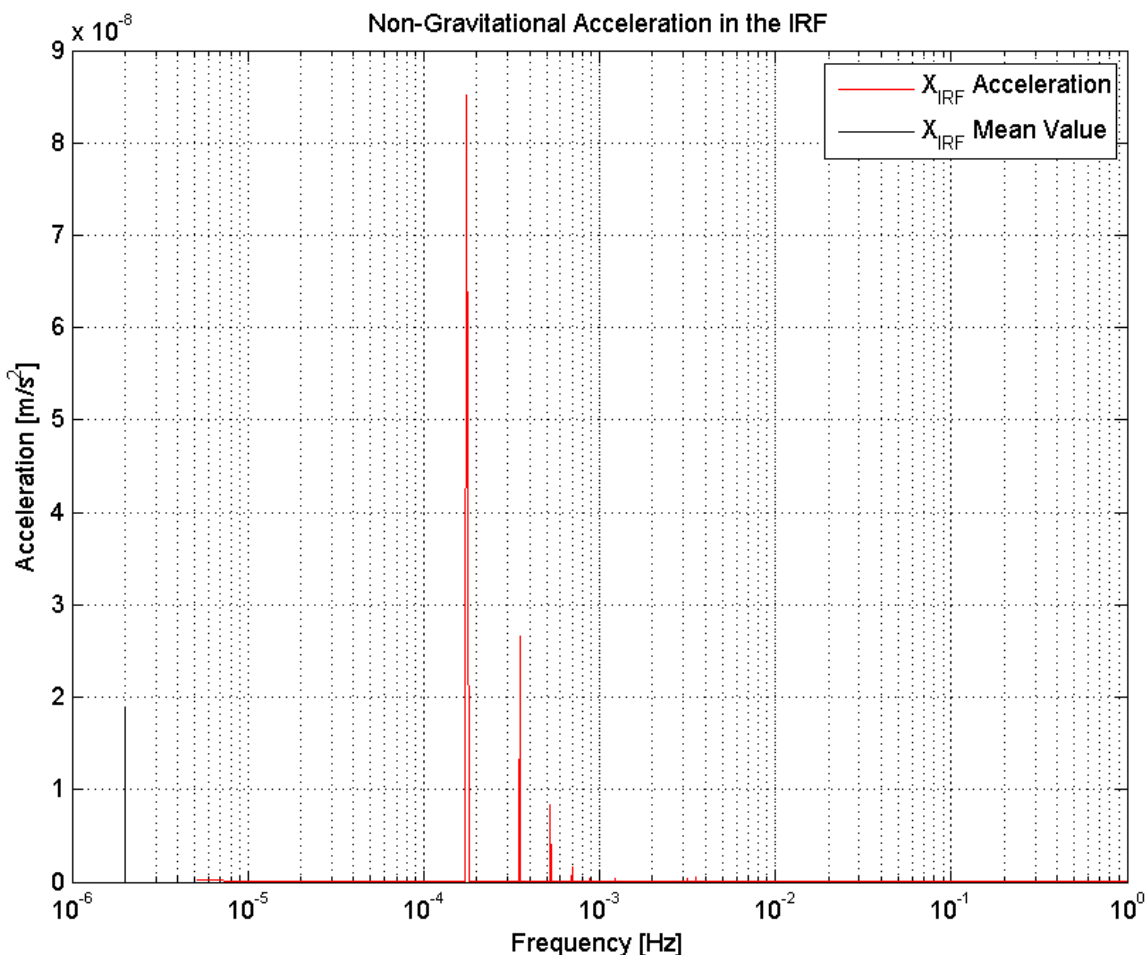


Figure 3.2-1: Non-gravitational acceleration in the IRF [X axis]

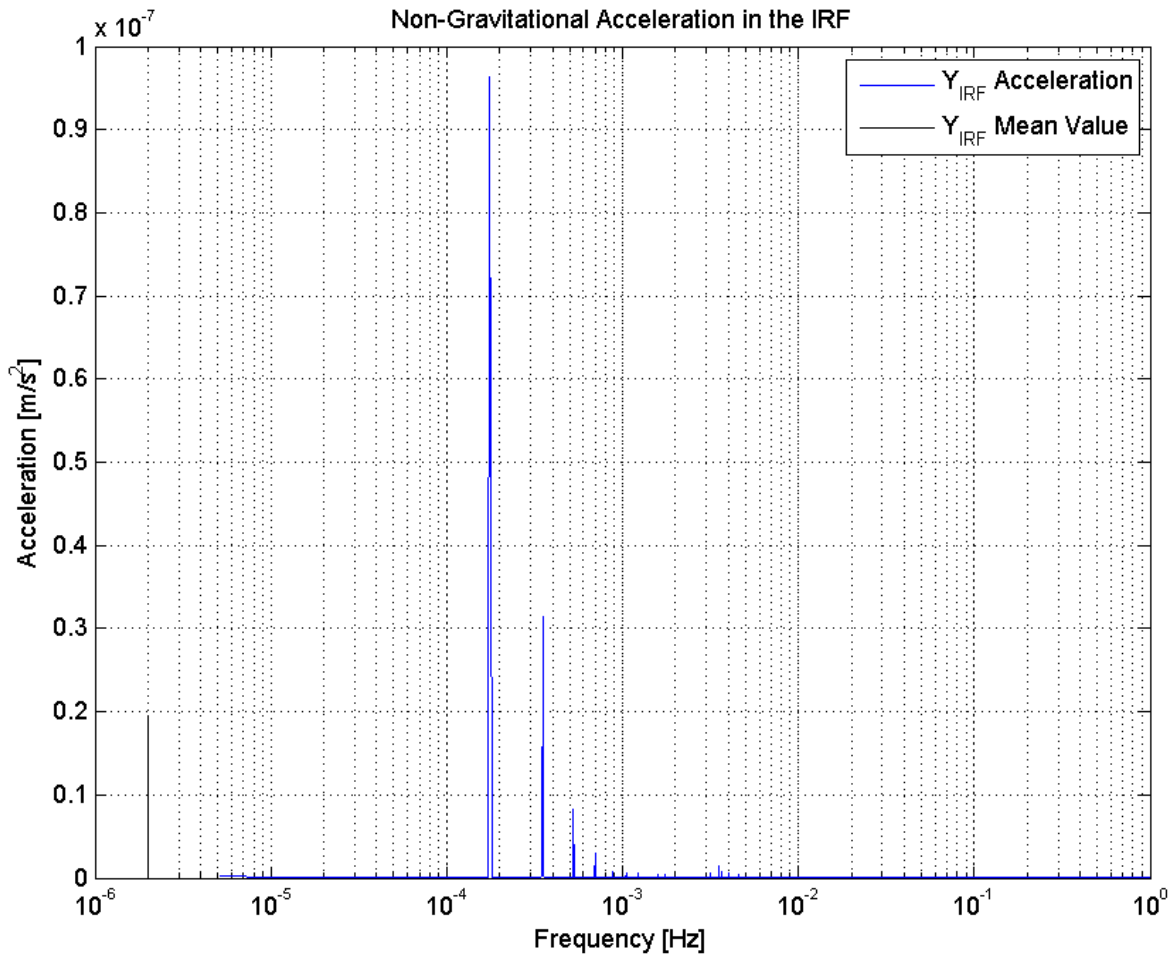


Figure 3.2-2: Non-gravitational acceleration in the IRF [Y axis]

The Figure 3.2-3, Figure 3.2-4 and Figure 3.2-5 provide the same previous overall non gravitational acceleration (environment disturbances and s/c-PGB suspension force) sensed from the satellite centre of mass wrt. LVLH frame.

The mean value of each acceleration component has been reported in the picture as a black line at the frequency $2 \cdot 10^{-6}$ Hz. In the LVLH frame, the main component of the external non gravitational acceleration is the mean term along Y. The EP violation signal consists of a test mass differential acceleration (displacement) along X.

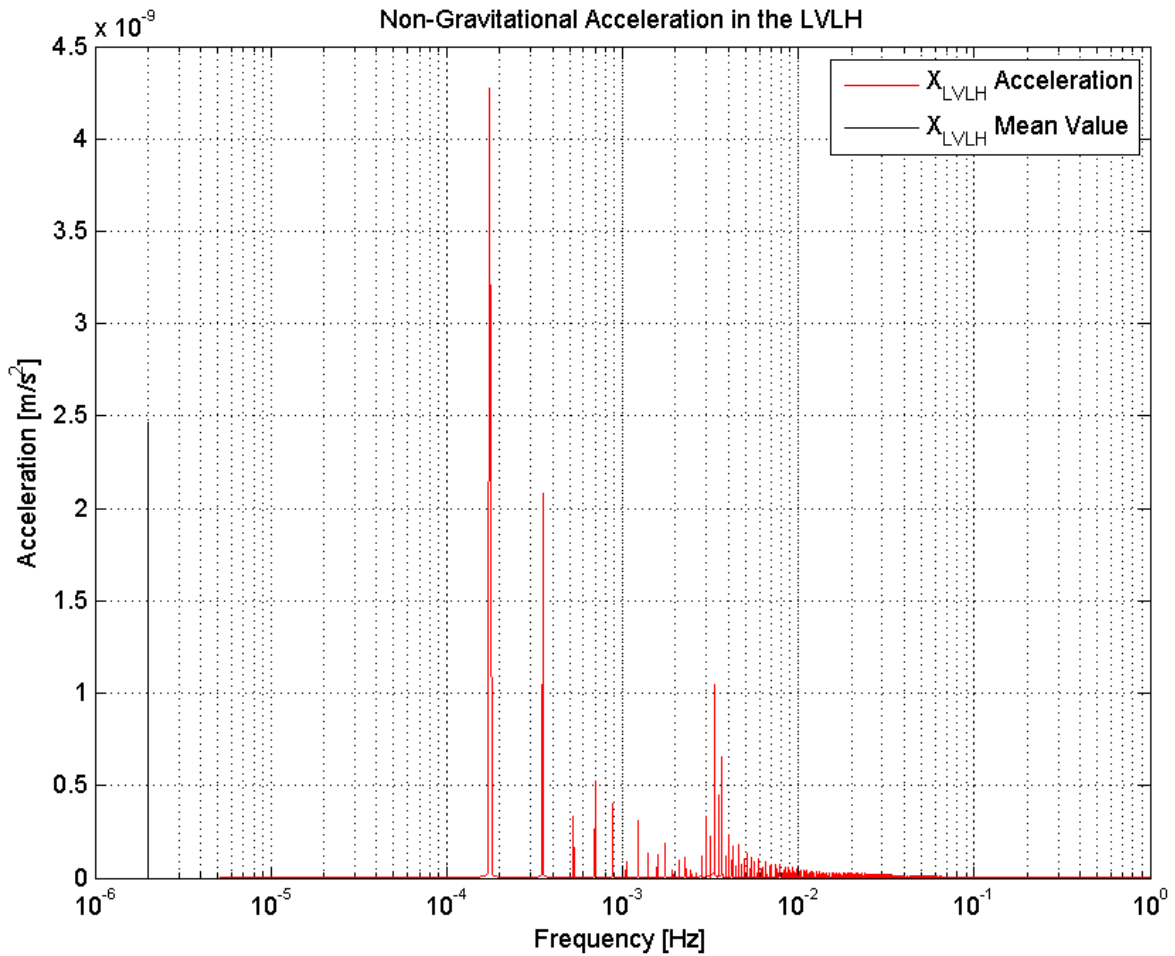


Figure 3.2-3: Non-gravitational acceleration in the LHLV reference frame [X axis]

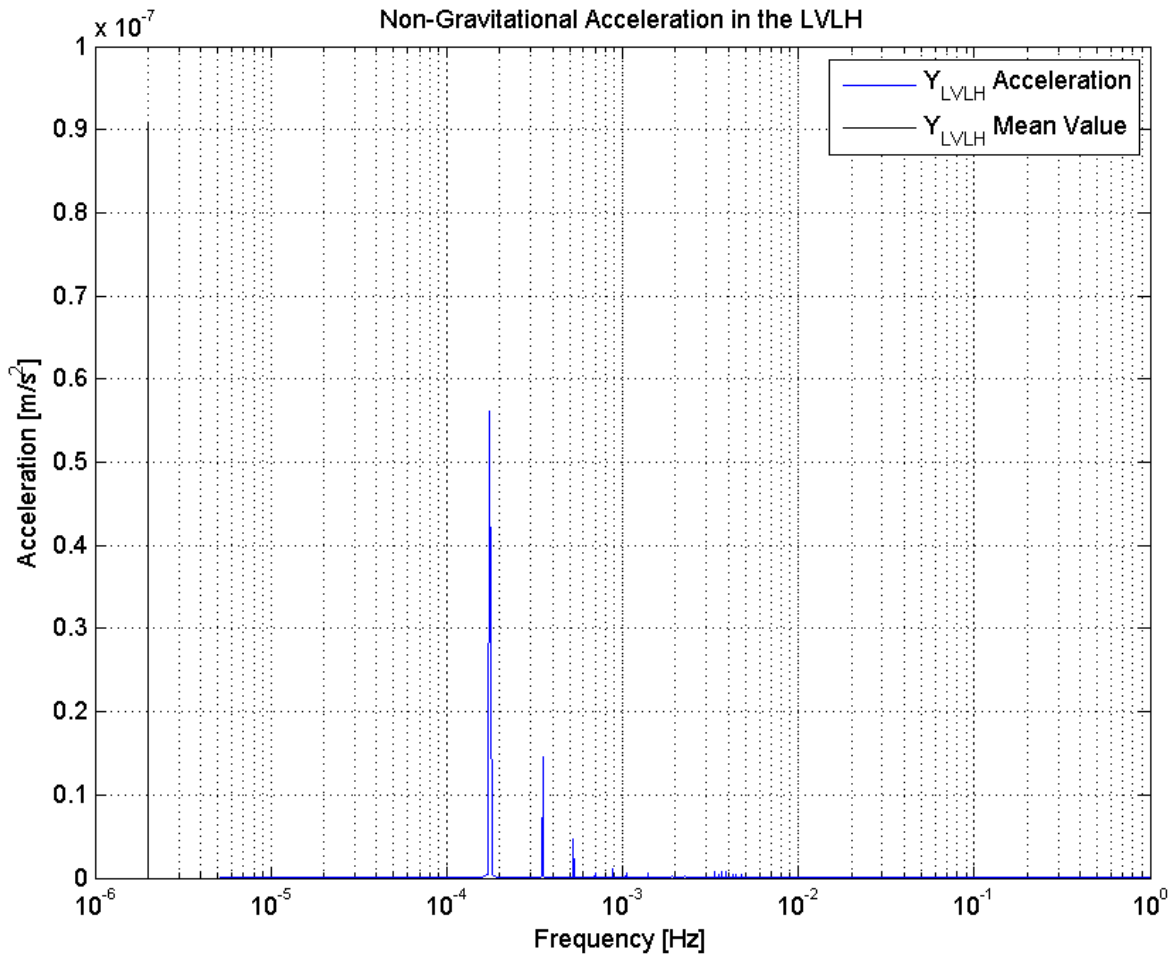


Figure 3.2-4: Non-gravitational acceleration in the LHLV reference frame [Y axis]

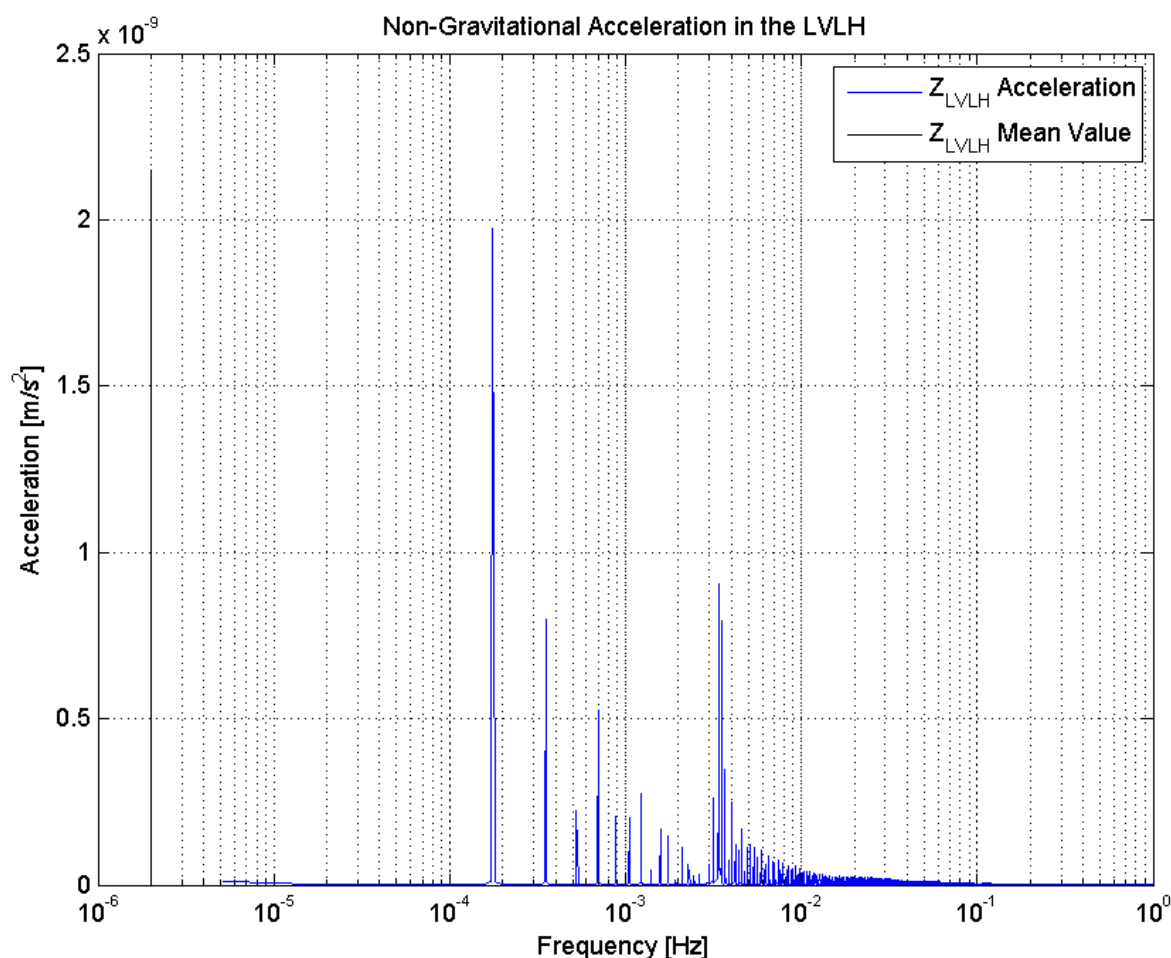


Figure 3.2-5: Non-gravitational acceleration in the LHLV reference frame [Z axis]

The Figure 3.2-6, Figure 3.2-7 and Figure 3.2-8 provide the same previous overall non gravitational acceleration (environment disturbances and s/c-PGB suspension force) sensed from the satellite centre of mass wrt. LVLH frame after the DFC compensation and the mechanical suspension rejection (CMRR).

The mean value (in the LVLH frame) of each acceleration component is not visible anymore, due to the DFC action and to the CMRR: $\text{mean}(a_{X_LVLH}) = 4.9 \cdot 10^{-19} \text{ m/s}^2$, $\text{mean}(a_{Y_LVLH}) = 1.8 \cdot 10^{-17} \text{ m/s}^2$, $\text{mean}(a_{Z_LVLH}) = 8.6 \cdot 10^{-14} \text{ m/s}^2$.

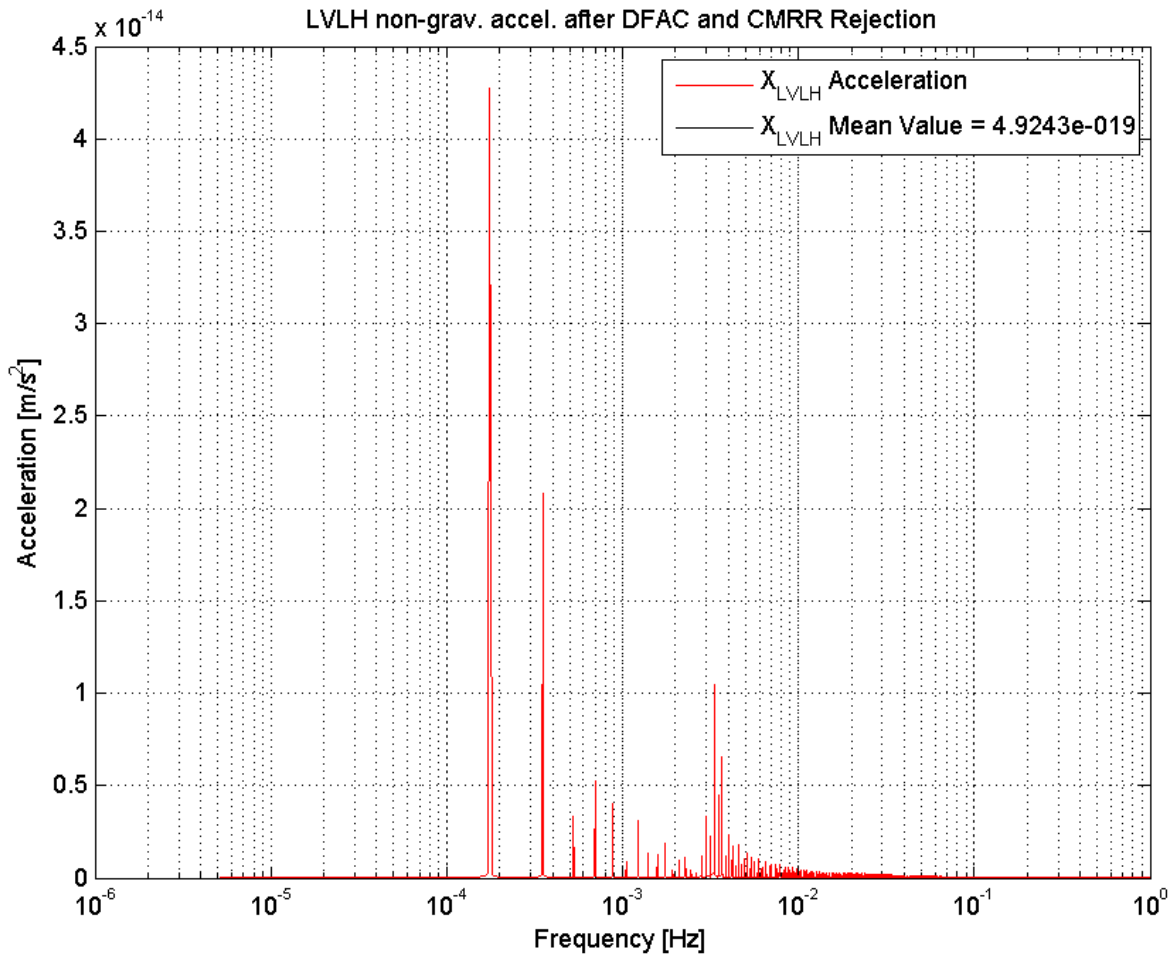


Figure 3.2-6: Non-gravitational acceleration in the LHLV reference frame after DFAC and Differential Accelerometer common mode rejection [X axis]

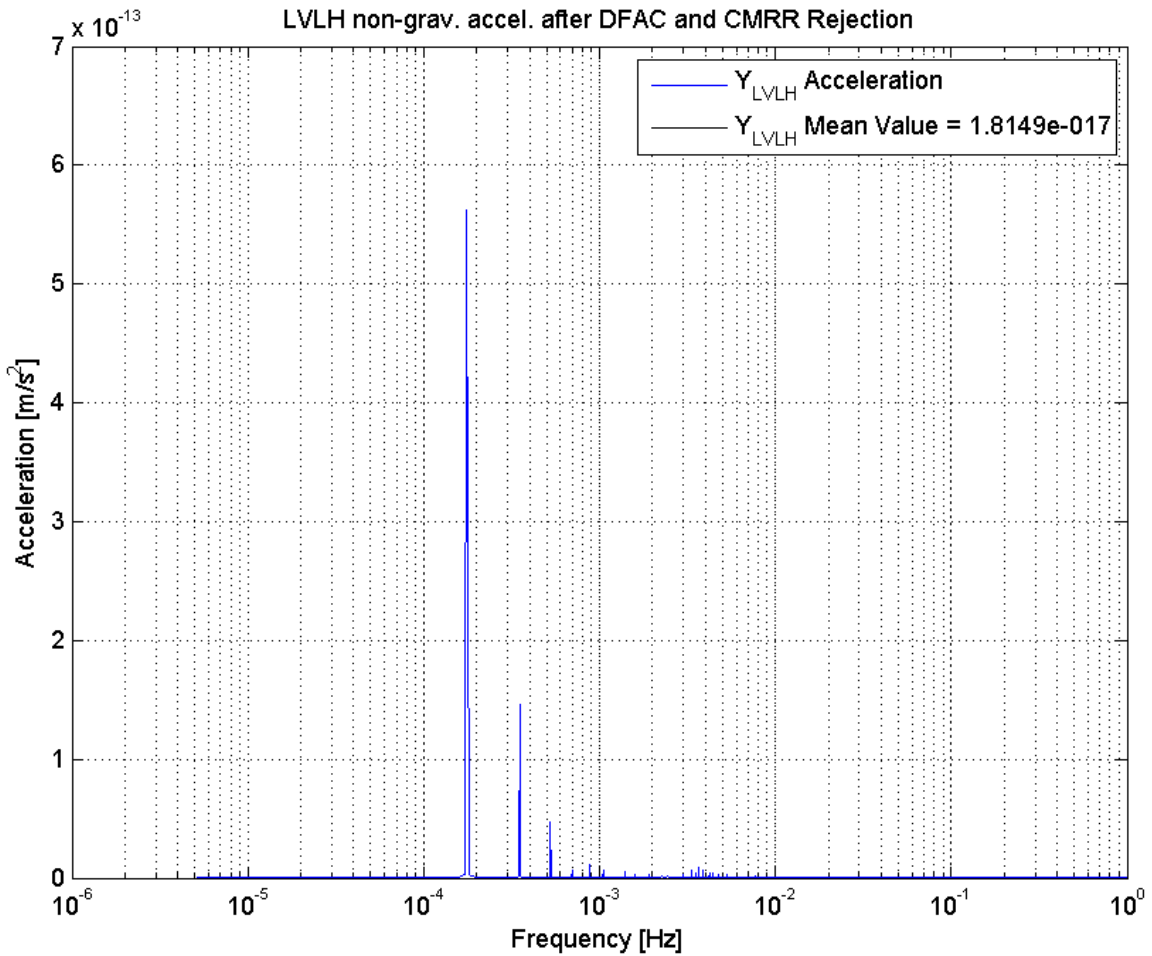


Figure 3.2-7: Non-gravitational acceleration in the LHLV reference frame after DFAC and Differential Accelerometer common mode rejection [Y axis]

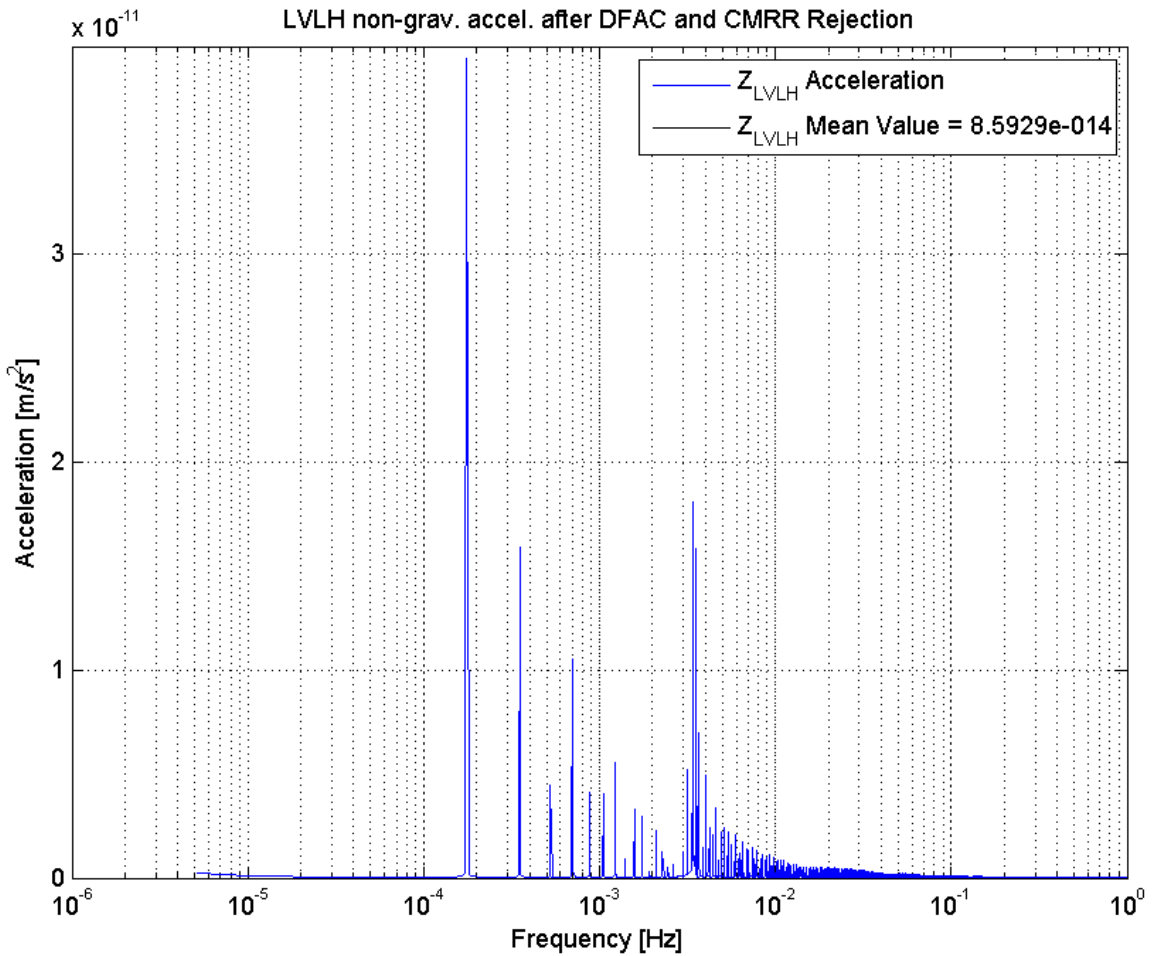


Figure 3.2-8: Non-gravitational acceleration in the LHLV reference frame after DFAC and Differential Accelerometer common mode rejection [Z axis]

3.3 Error Budget

The figures that follow provide the error budget of the systematic errors in graphical form.

Figure 3.3-1 shows the amplitude spectrum of the test masses differential displacement due to the main systematic errors vs. the simulated 0.6 pm EP violation signal. The amplitude of the error at the orbit frequency is smaller than the signal by a factor about 4. The closest error line is at twice the orbit frequency, with an amplitude one order of magnitude larger than the signal. This error can be easily distinguished from the signal during data processing, since the duration of each elementary experiment is about one week. The amplitude of the error at 4 times the orbit frequency is negligible. The error at the whirl frequency is easily removed during the synchronous demodulation of the post-processing.

Figure 3.3-2 shows a detailed view with all the main error terms. At twice the frequency of the EP signal, the errors due to magnetic coupling are negligible. At this frequency the main component of the displacement is due to the relative displacement of the test masses along the direction Z of the spin axis, which, through the gravity gradient, generates a displacement in the measurement plane. The relative displacement along Z is due mainly to the radiometric effect (worst case assumption for the residual pressure inside the PGB is made, and a better value is expected). Smaller contributions are due to the residual non-gravitational acceleration and to the differential thermal radiation emitted by the proof masses. At $4v_{EP}$, two different magnetic displacements induced, of negligible magnitude. The whirl and the Earth tides coupled with whirl generate three lines at frequencies v_{WHIRL} and $v_{WHIRL} \pm 2v_{EP}$. The three lines appear here as a single line at v_{WHIRL} due to their negligible separation in the logarithmic frequency scale. All three lines do not affect the signal detection, due to their large separation in frequency w.r.t. the orbit frequency.

Random noise is also available from the simulator. In GG the large mass of test bodies (10 kg) and the long period of their natural differential oscillations help in reducing thermal noise. Moreover, in supercritical rotation the relevant losses take place at the high spin frequency, at which they are small (as demonstrated by the losses measured with the laboratory prototype). Figure 3.3-3 shows a theoretical calculation of the thermal noise to be expected as the ultimate limitation.

The effects of electric charging are not modelled in the simulator. To reduce electric charging effects to negligible magnitude, one relies on gold coating of all the conductive surfaces and passive electric grounding of the test masses, as well as co-rotation of the test masses and the capacitance transducers. Moreover, surface charge patches can be measured in the GGG laboratory prototype, as it was recently shown.

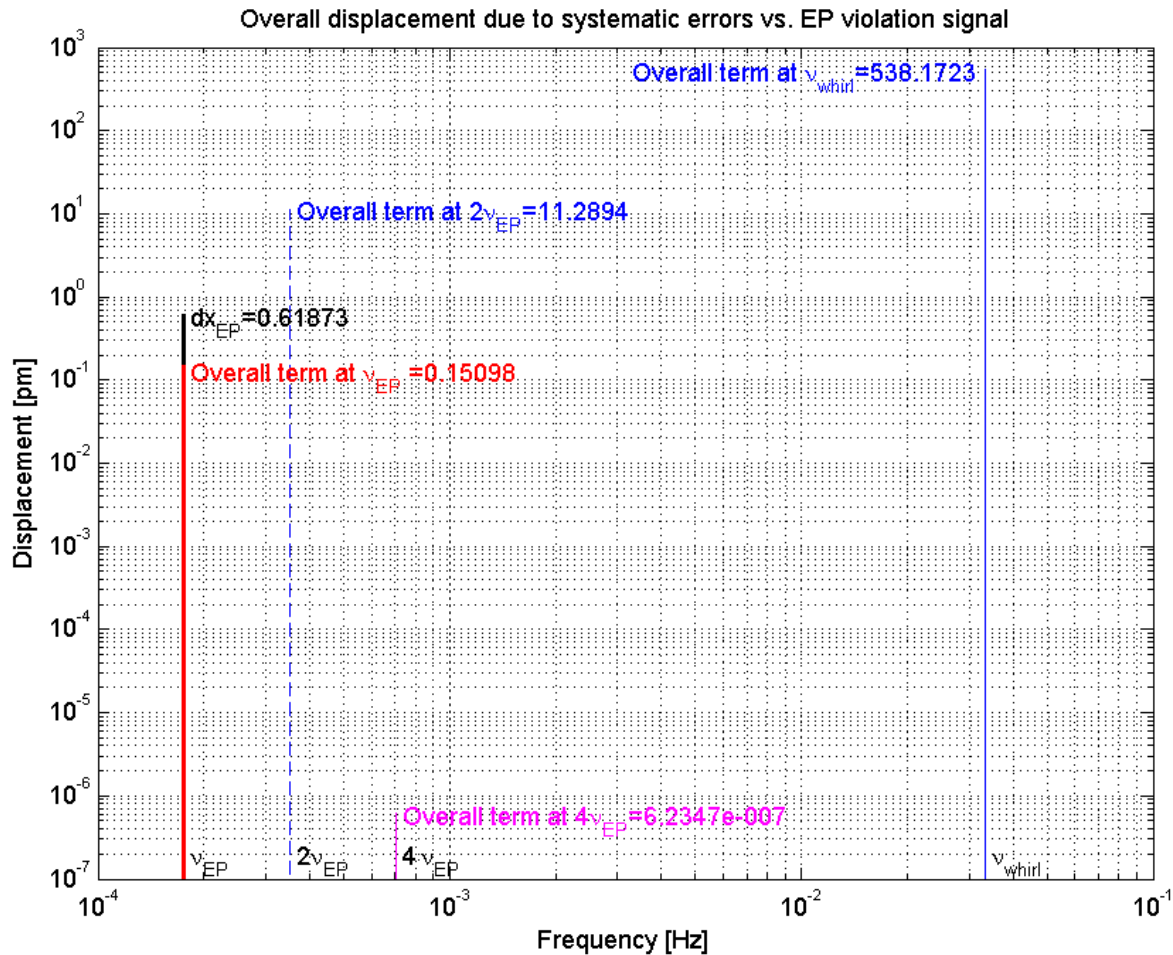


Figure 3.3-1: Amplitude Spectrum of the test masses differential displacement due to the main systematic errors vs. the target EP violation signal.

The target EP signal $\Delta x_{EP} = 0.61$ pm at the orbit frequency $\nu_{EP} = 1.7538 \times 10^{-4}$ Hz, w.r.t. the inertial reference frame IRF, is shown for comparison. The amplitude of the error at the orbit frequency is smaller than the signal by a factor about 4. The closest error line is at twice the orbit frequency, with an amplitude one order of magnitude bigger of the signal: this error can be easily distinguished from the signal during data processing, since the duration of each elementary experiment is about one week (the provided minimum step in frequency is about one millionth of Hz). The amplitude of the error at 4 times the orbit frequency is negligible. The error at the whirl frequency is easily removed during the synchronous demodulation of the post-processing.

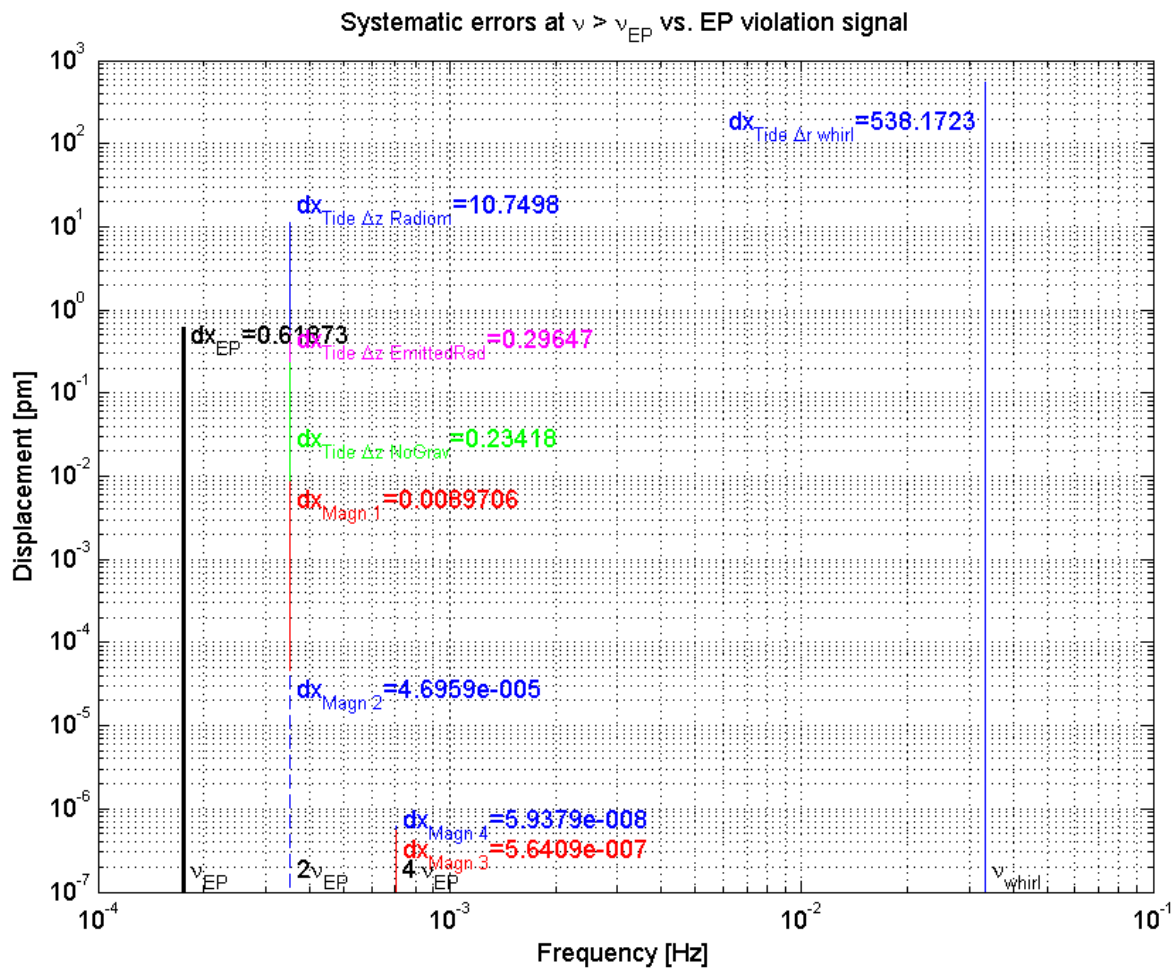


Figure 3.3-2: Detailed view of the Amplitude Spectrum of the main systematic errors.

The target EP violation signal $\Delta x_{EP} = 0.61$ pm at the orbit frequency is reported for direct comparison. At $2\nu_{EP}$ the errors due to magnetic coupling are negligible. At this frequency the main component of the displacement is due to the test masses differential displacement along the spin axis which through the gravity gradient generates a displacement in the plane of the science measurement. The differential displacement along z is due mainly to the radiometric effect (worst case assumption for the residual pressure inside the PGB is made, and a better value is expected). Smaller contributions are due to the residual s/c non-gravitational acceleration and to the proof masses emitted radiation. At $4\nu_{EP}$, the two different magnetic induced displacements are negligible. The whirl and the Earth tides coupled with whirl generate three lines at frequencies ν_{whirl} and $\nu_{whirl} \pm 2\nu_{EP}$. The three lines appear here as a single line at whirl ν due to their negligible separation in the logarithmic frequency scale. All three lines do not affect the signal detection, due to their large separation in frequency w.r.t. the orbit frequency.

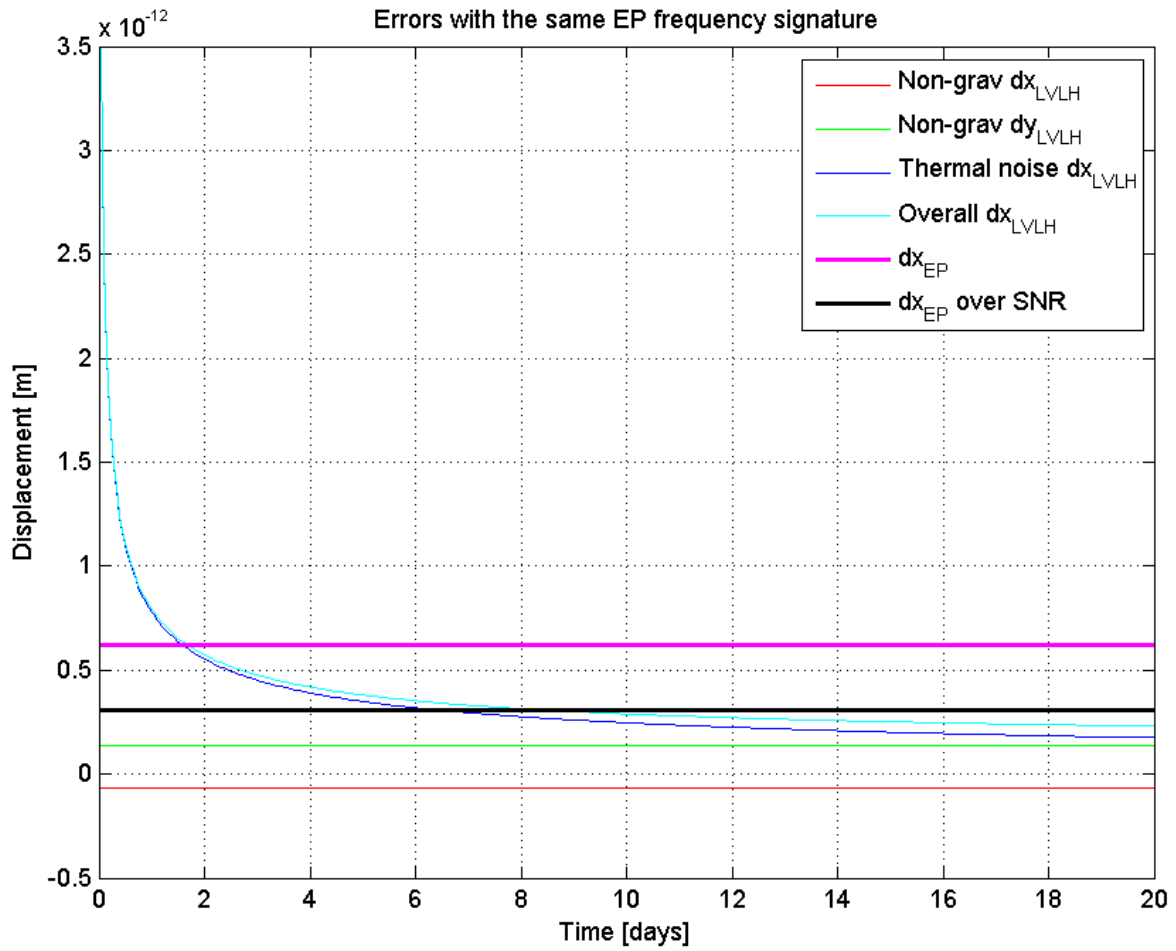


Figure 3.3-3: Magnitude of the errors with the same frequency signature as the EP violation signal, as function of integration time.

CONTROLLED DISTRIBUTION



REFERENCE : SD-RP-AI-0620

DATE : June 09

ISSUE : 02 **PAGE :** 21/21

END OF DOCUMENT

THALES

All rights reserved, 2007, Thales Alenia Space

CONTROLLED DISTRIBUTION

M032-EN

100181547K-EN